Terminal attack trajectories of peregrine falcons are described by the proportional navigation guidance law of missiles

Caroline H. Brighton[a], Adrian L. R. Thomas[a], and Graham K. Taylor[a,1]

[a]Department of Zoology, University of Oxford, OX1 3PS, United Kingdom

Edited by David Lentink, Stanford University, Stanford, CA, and accepted by Editorial Board Member Neil H. Shubin October 25, 2017 (received for review August 18, 2017)

The ability to intercept uncooperative targets is key to many diverse flight behaviors, from courtship to predation. Previous research has looked for simple geometric rules describing the attack trajectories of animals, but the underlying feedback laws have remained obscure. Here, we use GPS loggers and onboard video cameras to study peregrine falcons, *Falco peregrinus*, attacking stationary targets, maneuvering targets, and live prey. We show that the terminal attack trajectories of peregrines are not described by any simple geometric rule as previously claimed, and instead use system identification techniques to fit a phenomenological model of the dynamical system generating the observed trajectories. We find that these trajectories are best—and exceedingly well—modeled by the proportional navigation (PN) guidance law used by most guided missiles. Under this guidance law, turning is commanded at a rate proportional to the angular rate of the line-of-sight between the attacker and its target, with a constant of proportionality (i.e., feedback gain) called the navigation constant (N). Whereas most guided missiles use navigation constants falling on the interval $3 \leq N \leq 5$, peregrine attack trajectories are best fitted by lower navigation constants (median $N < 3$). This lower feedback gain is appropriate at the lower flight speed of a biological system, given its presumably higher error and longer delay. This same guidance law could find use in small visually guided drones designed to remove other drones from protected airspace.

peregrine falcon | pursuit | guidance law | system identification | proportional navigation

The success of any aerial predator hinges on its ability to steer a collision course to its prey, which previous work has explored by looking for simple rules describing the geometry of an attack (1–11). For example, many predators are said to hold the geographic direction of their target constant on approach. This geometry guarantees interception, but describes pattern, not process, being only the idealized outcome of some underlying guidance law by which sensory feedback is used to command body accelerations (12). Guidance laws have previously been fitted to the flight trajectories of chasing flies (13–16), where the picture is complicated by the fact that the pursuer is not necessarily trying to intercept the object of its territorial or courtship behavior (see also refs. 17–19). Guidance laws have also been fitted to the flight trajectories of pigeons avoiding obstacles (20), modeled as a piecewise target-aiming behavior at gaps identified post hoc from the observed trajectory. These examples contrast with the case of aerial predation, for which the objective of the behavior is clear, but for which the underlying guidance laws remain obscure. Here, we analyze the aerial attack behaviors of peregrines, *Falco peregrinus*, dynamically, using GPS data supported by onboard video to identify a simple guidance law capable of generating the trajectories observed during the terminal phase of an attack.

Previous studies have described the target-oriented behaviors of animals using three simple geometric rules, each defined by the constancy of one of two angles characterizing the 2D geometry of a chase: the line-of-sight angle (λ), defined as the compass bearing of the line-of-sight from pursuer to target; and the deviation angle (δ) between the line-of-sight and the pursuer's velocity vector. Under a first geometric rule (Fig. 1*A*), the pursuer flies directly at its target at all times (t), producing a pure pursuit course defined by the rule $\delta(t) = 0$. Pure pursuit has been described in hawks attacking stationary targets (10), flies chasing mates (13–16), fish catching sinking food (21), beetles running after targets (22, 23), and bees landing on a moving platform (24). Under a second geometric rule (Fig. 1*B*), the pursuer directs its velocity at a nonzero lead angle α ahead of the line-of-sight, producing a deviated pursuit course defined by the rule $\delta(t) = \alpha$. Deviated pursuit has been hypothesized in falcons on the basis of their visual anatomy (7, 8), but behavioral evidence is lacking (9). Under a third geometric rule (Fig. 1*C*), seen in dragonflies (1–5), robber flies (6), falcons (9), hawks (10), and bats (11), the pursuer keeps its target on a constant compass bearing. This results in a parallel navigation course defined by the rule $\lambda(t) = \lambda(0)$, and leads incidentally to a form of motion camouflage, because the pursuer appears stationary against a distant background (2, 25, 26) [also called constant absolute target direction (9–11) or constant bearing angle (6)]. Missile engineers designed guidance laws to implement these geometric rules decades ago (12), but it is not yet known how they are implemented by aerial predators.

Past research has tried to relate the curved geometry of raptor attack trajectories to the constraints imposed by their visual anatomy (7–9). Birds vary considerably in the extent of their eye movements, but these are limited in falcons, which have two acute

Significance

Renowned as nature's fastest predators, peregrines are famous for their high-speed stooping and swooping attack behaviors. We used miniature GPS receivers to track peregrines attacking dummy targets thrown by a falconer or towed by a drone and fitted a simulation describing the dynamics of the guidance system used in interception. We collected onboard video giving a falcon's-eye view of the attacks and used this to validate our conclusions for attacks on live targets. Remarkably, we find that the terminal attack trajectories of peregrines are described by the same feedback law used by visually guided missiles, but with a tuning appropriate to their lower flight speed. Our findings have application to drones designed to remove other drones from protected airspace.

Author contributions: A.L.R.T. and G.K.T. designed research; C.H.B. and G.K.T. performed research; C.H.B. and G.K.T. analyzed data; and C.H.B. and G.K.T. wrote the paper.

The authors declare no conflict of interest.

This article is a PNAS Direct Submission. D.L. is a guest editor invited by the Editorial Board.

Data deposition: All GPS and video data have been uploaded to Dryad Digital Repository (https://doi.org/10.5061/dryad.md268).

[1]To whom correspondence should be addressed. Email: graham.taylor@zoo.ox.ac.uk.

This article contains supporting information online at www.pnas.org/lookup/suppl/doi:10.1073/pnas.1714532114/-/DCSupplemental.

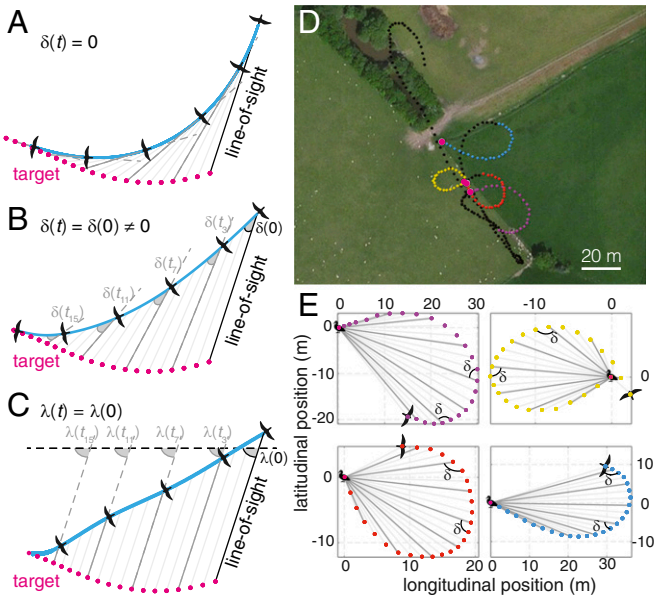

Fig. 1. Three geometric rules classically used to describe aerial attack behaviors (*A*–*C*), compared with actual GPS track for live attack on a mallard (*D* and *E*). Straight lines mark the line-of-sight from attacker to target at regular time intervals. (*A*) Pure pursuit. (*B*) Deviated pursuit. (*C*) Parallel navigation. (*D*) Attack on mallard comprising aerial chase followed by four low-altitude swoops (colored points). (*E*) Geometric analysis of four swoops at mallard. Note the constancy of the deviation angle (δ) in *A* and *B* and the constancy of the line-of-sight angle (λ) in *C*; neither the deviation angle nor the line-of-sight angle was held constant in the attacks on the mallard (*E*), so the actual behavior is not described by any simple geometric rule.

zones in each eye: a forward-facing shallow fovea and a laterally directed deep fovea (27). The former is used to inspect nearby targets, but raptors typically look laterally at distant targets, leading Tucker (7) to propose that the deep fovea would be used to target aerial prey. Tucker further proposed that a falcon would hold its head symmetrically for streamlining in a stoop, leading to the hypothesis that it would naturally fly a deviated pursuit course with a lead angle $\alpha \approx 45°$, equal to the azimuthal angle of the deep fovea (7). Under this hypothesis, the geometry of a falcon's attack trajectory emerges from the kinematic constraints imposed by its anatomy and aerodynamics, rather than from any underlying feedback law. Recent observational studies using head-mounted video cameras (9) have cast doubt on the supposition that the deep fovea is used to target aerial prey, as the target's inferred position on the retina is nearer to that of the shallow fovea (9). Furthermore, it has been suggested that the apparent target motion in these videos is more consistent with the use of parallel navigation than deviated pursuit (9). It therefore appears that the curved attack trajectories of falcons cannot be explained away as an emergent property of their visual anatomy. On the contrary, it may only be possible to understand the functional significance of this visual anatomy given a suitable model of their guidance.

The guidance systems of most modern missiles use a guidance law called proportional navigation (PN), in which turning is commanded at a rate $\dot{\gamma}$ proportional to the rotation rate of the line-of-sight (i.e., the line-of-sight rate, $\dot{\lambda}$), such that

$$\dot{\gamma}(t) = N\dot{\lambda}(t) \quad [1]$$

where N is termed the navigation constant and falls on the interval $3 \leq N \leq 5$ in missiles (12). (Note that PN refers specifically to the guidance law stated in Eq. **1** and is distinct from proportional control.) Changes in the line-of-sight can be produced by motion of either the target or attacker, so PN commands turning toward the target even when it is stationary, except in the degenerate case that the attacker is already flying directly at its target. Moreover, the same guidance law can be generalized to the 3D case and is capable of producing any of the three attack geometries described above (*SI Appendix*). When N is high, the commanded turn rate nullifies the line-of-sight rate, so that $\dot{\lambda}(t) \approx \dot{\lambda}(0)$, producing a parallel navigation course (Fig. 1*C*). When $N = 1$, the commanded turn rate matches the line-of-sight rate, so that $\dot{\delta}(t) = \dot{\delta}(0)$, producing a pure or deviated pursuit course (Fig. 1 *A* and *B*), according to the initial conditions on $\dot{\delta}(0)$. While there are plausible attack geometries that cannot be produced by PN, the same guidance law produces a continuum of other trajectories at intermediate N (12). Other guidance laws are possible. Most are simply PN variants (12), but a different and direct way of implementing pursuit would be to command turning in proportion to the deviation angle δ, with $\dot{\gamma}(t) = -K\delta(t)$, where K is a positive constant. This proportional pursuit (PP) guidance law drives the deviation angle to zero, such that $\delta(t) \approx 0$, but is easily modified to implement deviated pursuit (*SI Appendix*, Eq. **S4**). PP guidance differs fundamentally from PN at $N = 1$, which produces a pursuit course by holding δ unchanging, rather than by driving δ to any particular value. PP guidance has been used successfully to model chases in flies (13–16) and has also found use in some early guided missiles, but is not widely used today. This is not surprising given that PN can be shown to be optimal against nonmaneuvering targets and near-optimal against maneuvering ones (12). The simplicity, efficacy, and generality of PN make it an excellent candidate for explaining how animals intercept stationary and maneuvering targets (3, 4, 6, 12, 28), but this has not been shown empirically.

Peregrines Use a Diverse Range of Attack Behaviors

We challenged $n = 8$ captive peregrines to attack a food lure resembling a winged prey item, which was thrown upward by the falconer (stationary targets: 26 flights for $n = 3$ birds in 2012/13; Movie S1) or towed spinning through the air by a small remotely piloted aircraft (maneuvering targets: 35 flights for $n = 5$ birds in 2014/16; Movies S2 and S3). We did not encourage hunting, but our video data revealed 12 opportunistic hunts and 2 territorial interactions with live targets (Figs. 2 and 3 and Movies S4–S6). No live hunt ended in a kill, but this is not necessarily surprising, as reported success rates for wild peregrines range upward from 8% (29), and the binomial probability of experiencing a run of 12 unsuccessful hunts at an 8% success rate is $P = 0.37$. Peregrines are known for their high-speed, gravity-assisted stoops, but many or most attacks over open habitats involve level chases or low-altitude swoops at sitting or swimming prey (29–31). Our birds used a similarly diverse range of behaviors: Only 4 (33%) of the 12 live hunts began with a stoop; the other 8 (67%) began as level chases, including 1 (8%) from a perch. All 35 flights at maneuvering targets began as level chases, and of the 26 flights at stationary targets, 9 (35%) began with a gravity-assisted stoop and 5 (19%) with a low-altitude swoop; the other 12 (46%) began as level chases, including 3 (12%) from a perch. If the initial attack was unsuccessful, then this was usually followed by a series of swoops (Fig. 1*D*), as is also typical of natural hunting behavior.

Peregrine Terminal Attack Trajectories Are Not Described by Any Single Geometric Rule

The birds often made more than one attack pass before capturing their target, and we treated these separately in the analysis below. In total, we obtained high-quality GPS data from 33 passes at stationary targets and 22 passes at maneuvering targets (*SI Appendix*). These include five passes at a mallard, *Anas platyrhynchos*, that landed to take cover (Fig. 1*E*), allowing us to identify its position as for other stationary targets. The deviation angle δ varied continuously during these attacks (Fig. 1*E* and *SI Appendix*, Fig. S1), except in a few degenerate cases involving straight flight at a stationary target, for which $\delta(t) \approx 0$, as in pure pursuit. The GPS data showed that the line-of-sight angle λ also varied continuously, but became more constant on

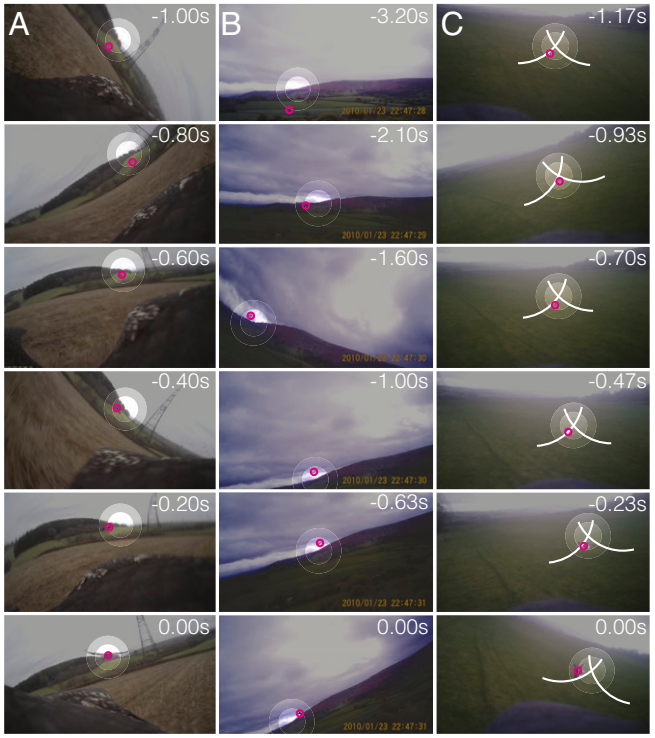

Fig. 2. Video sequences from cameras worn dorsally by peregrines chasing live targets (magenta): corvids *Corvus spp*. (*A* and *B*; Movies S5 and S6) and mallard (*C*; Movie S4). All frames have been uniformly darkened apart from within a circular mask subtending 6° (inner circle) or 10° (outer ring). Each mask is centered on a consistently identifiable reference point on the horizon or at the intersection of a pair of circular arcs (white lines) centered on two such points. This ensures that the mask is located on a constant compass bearing, regardless of how the attacker behaves or how the camera moves (*SI Appendix*). Any drift in the line of sight is therefore measured by the target's movement with respect to the mask. Because the target (magenta) remains within the 6° diameter of the inner circle of the mask, it follows that the line of sight is held steady to within ±3° over the last 1–2 s of each attack.

final approach (Fig. 1*E* and *SI Appendix*, Fig. S1). This was confirmed by the videos of attacks on live targets, which showed the line-of-sight becoming steady to within ±3° over the last 1–2 s of each attack (Fig. 2). The geometry of our peregrines' attack behaviors was therefore fundamentally different from the deviated pursuit strategy proposed by Tucker et al. (7, 8) and more complex than the parallel navigation strategy proposed by Kane et al. (9, 10). In summary, there is no evidence that peregrine attack trajectories are described by any single geometric rule (cf. refs. 7–10), but they are consistent with the use of a guidance law that tends to bring the attacker onto a parallel navigation course on final approach. PN is the obvious candidate, which we test formally below.

Peregrine Terminal Attack Trajectories Are Well Modeled by a PN Guidance Law

Our peregrines flew an almost planar attack trajectory against stationary targets, but only did so for maneuvering targets when engaged in a level chase. Hence, as most of the attack trajectories were quite shallow, we first undertook a 2D system identification analysis of the horizontal components of the trajectories, before undertaking a 3D analysis of any passes with an altitudinal range ≥10 m over the section simulated in 2D. For each attack pass, we simulated the trajectory that would have emerged under PN or PP guidance at the best-fitting value of the guidance constant N or K in nominally lag-free conditions (*SI Appendix*). We ran these simulations given knowledge of the initial position and velocity of the attacker, the time history of the attacker's groundspeed, and the time history of the target's position. We used the guidance law to simulate all of the changes in the attacker's flight direction, but forced the attacker's speed to match what we had measured empirically. Matching the speed in this way is essential to ensuring proper determination of the line-of-sight rate and ensures that any prediction error is wholly attributable to error in the simulated time history of the attacker's turning. We assumed that the actual acceleration of the attacker in our simulations was the same as the commanded acceleration (i.e., we assumed that the attacker could meet its acceleration demand), which is reasonable because any guidance model that fits the data must by definition be feasible within the actual biomechanical constraints on the system.

We identified the best-fitting values of N and K separately for each attack pass by minimizing the overall prediction error, defined as the mean absolute distance between corresponding sample points on the simulated and measured trajectories. This system identification approach accommodates variability in the guidance parameters N and K, which could be expected under optimal guidance (see below), but risks overparameterization. It is important to note, therefore, that our subsequent statistical inferences were based on: (*i*) a contrastive test of the fit of two alternative guidance laws, each with one fitted guidance parameter per pass; and (*ii*) an analysis of the population properties of the fitted guidance parameters, which were expected to take values within a particular range (see below). Since there was no prior way of knowing when an attacker first initiated its target-oriented behavior, we ran simulations beginning from all possible start times ≥2.0 s before intercept and reported the longest simulation for which the mean prediction error was less than some predetermined threshold as a percentage of the total distance flown (Fig. 3). In other words, we fitted the terminal phase of each attack pass, starting the fit from as far back as would meet the specified error tolerance. Simulations of the same trajectory begun closer to the point of intercept usually had a lower mean prediction error. The length of the fit was therefore the key metric for assessing how well a given model described the data, both in an absolute sense and relative to any alternative. However, because the guidance laws that we compared were only used to predict the turning behavior of the attacker, it follows that a fitted trajectory is only informative if it involves a substantial amount of turning: Straight trajectories can be fitted well under either guidance law, so are not informative.

The PN simulations modeled a significantly higher proportion of passes at 1.0% error tolerance than did the PP simulations (46 vs. 35 of 55 passes; exact McNemar's test: two-tailed $P = 0.001$; *SI Appendix*, Table S1). Moreover, for those passes that could be modeled successfully by both guidance laws, the PN simulations

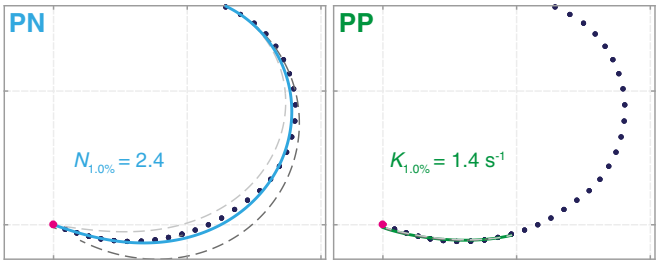

Fig. 3. Representative GPS track for peregrine (blue points) attacking stationary target (magenta points), overlain with best-fitting 2D simulations under PN (blue line) and PP (green line). Simulations start from the earliest point for which prediction error is <1.0% of total distance flown; $N_{1.0\%}$ and $K_{1.0\%}$ denote the best-fitting values of the respective guidance constants at this error tolerance. Dashed lines indicate sensitivity of the simulation by increasing (light gray) or decreasing (dark gray) the fitted value of the guidance constant ±10%. In most cases, the PN simulation was highly sensitive to the value of N (sensitivity ratio for this simulation: 42.8), which should therefore have been reliably estimated by our method. The PP simulations did not fit much of the data well and were often quite insensitive to the value of K (see *SI Appendix*, Table S2 for results for all passes). Grid lines are at 10-m spacing.

fitted a significantly longer duration of flight (median duration: 4.9 s; first, third quartiles: 3.3, 8.8 s) than did the PP simulations (sign test on 27 untied differences: two-tailed $P = 0.0003$). We therefore concluded that PN was much the better supported of the two guidance laws we tested (see also Fig. 3) and present only the results of the PN simulations hereon. In aggregate, our PN simulations modeled >4.2 km of flight at 1.0% error tolerance (*SI Appendix*, Table S1), fitting long sections of flight against both stationary (median simulation length: 47 m; first, third quartiles: 31, 71 m) and maneuvering (median simulation length: 114 m; first, third quartiles: 45, 200 m) targets. Although our PN simulations could not model all of the attack passes at 1.0% error tolerance, this reflects the stringency of the error threshold chosen in advance of our analysis, coupled with our requirement to model ≥2 s of flight.

A few of the attacks involved long sections of nearly straight flight toward the target, but while these were consistent with the use of PN, the guidance dynamics were not strongly excited in these degenerate cases, making parameter estimation unreliable (*SI Appendix*, Table S2). We therefore focused our reporting on the more informative subset of attacks involving the most turning, which we assessed by ranking the trajectories according to aspect ratio. Fig. 4 presents the 15 trajectories involving the most turning (see *SI Appendix*, Figs. S2 and S3 for the rest), from which it is clear that PN guidance is capable of generating most of the turning behavior that we observed. For example, the paths of increasing radius that the peregrines followed toward stationary targets all belong to the family of curves generated naturally by the dynamics of PN guidance (Fig. 4 *F*–*O*). Moreover, whereas the three geometric rules only make sense when an attacker is already closing range on its target, PN can also generate the turning behavior observed when an attack is started with the attacker flying away from its target (Fig. 4 *I*–*M*). PN guidance can even generate a hairpin turn that one of the peregrines made after missing a maneuvering target (Fig. 4*A*). Our simulations performed comparably well in 3D at an equivalent 1.2% error tolerance for those attacks involving substantial changes in altitude (Fig. 5), accurately describing the curved descent of the longest gravity-assisted stoop that we observed (Fig. 5*B*). No geometric rule could possibly describe this breadth of behavior, and indeed the decreasing radius of the spiraling flight path predicted under Tucker's model of deviated pursuit in falcons (7) is opposite to the increasing radius of the curves that we observed (Fig. 4).

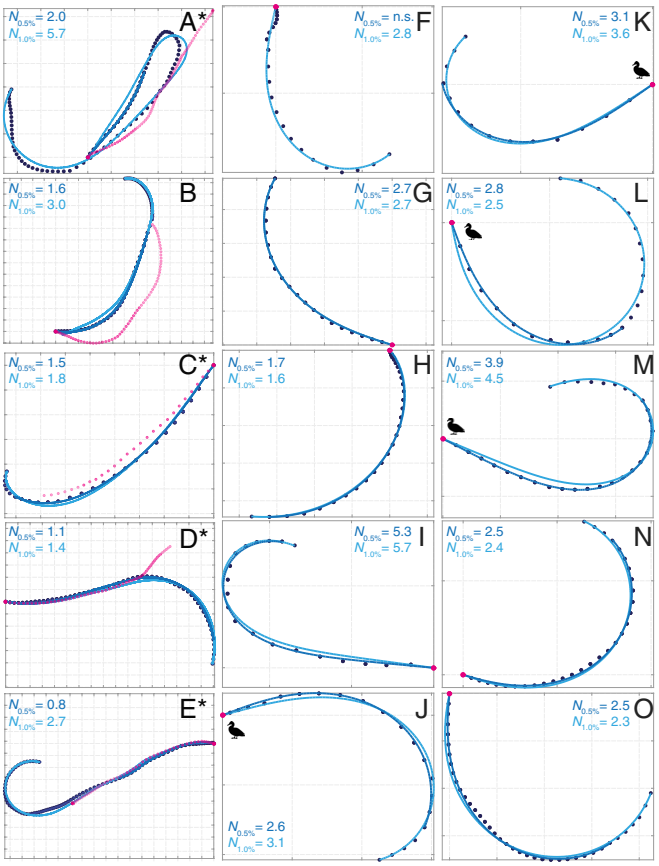

Fig. 4. GPS tracks for peregrines (blue points) attacking maneuvering (*A*–*E*) or stationary (*F*–*O*) targets (magenta points), overlain with best-fitting 2D simulations under PN guidance (blue lines). Duck icons indicate live targets (cf. Fig. 1*E*). Simulations start from the earliest point for which the prediction error is <0.5% (dark blue) or <1.0% (light blue) of the distance flown; $N_{0.5\%}$ and $N_{1.0\%}$ denote the best-fitting values of N at each error tolerance. n.s., no simulation. The 15 trajectories involving the most turning are plotted here; see *SI Appendix*, Figs. S2 and S3 for the 31 other trajectories fitted at 1.0% error tolerance. Starred trajectories are simulated in 3D in Fig. 5. Grid lines are at 10-m spacing.

Sensitivity of Method and Robustness of Simulations

We verified the sensitivity of our system identification analysis by computing the percentage change in the mean absolute distance between the simulated and measured trajectories in response to a ±10% change in their fitted values of N (Fig. 3), quantifying the sensitivity as the ratio of these percentage changes (sensitivity ratios in *SI Appendix*, Table S2). The match between the simulated and measured trajectories was highly sensitive to the value of N (median sensitivity ratio: 3.5; upper, lower quartiles: 1.4, 28.5), so for a given start point, the best-fitting value of N was usually well defined (Fig. 3). The best-fitting value of N is itself sensitive to the initial conditions, however, and so depends on the selected start point of the simulation. The start points of our simulations were determined by our choice of error tolerance, but the population properties of the fitted values of the navigation constants were robust to this: Values of N fitted to shorter lengths of flight at 0.5% error tolerance (median $N_{0.5\%}$: 2.5; first, third quartiles: 1.5, 3.9) did not differ systematically (sign test on 22 untied differences: $P = 0.83$) from values of N fitted to longer lengths of flight at 1.0% error tolerance (median $N_{1.0\%}$: 2.6; first, third quartiles: 1.5, 3.2) (Fig. 4 and *SI Appendix*, Table S2). This presumably reflects the fact that the terminal phase of an attack is short enough for the guidance dynamics to be treated as time-invariant, even if parametric variation in the guidance dynamics becomes apparent over the longer time intervals between passes.

The preceding simulations were fitted assuming nominally lag-free guidance, notwithstanding the timing uncertainty of ±0.1 s implicit in aligning our 5-Hz GPS measurements to the point of capture. To verify the robustness of our simulations to this uncertainty, which precludes reliable estimation of the inevitable sensorimotor delay, we reran the PN simulations after lagging the line-of-sight rate fed back to command turning by a delay equivalent to one GPS sample interval. Adding this explicit 0.2-s delay worsened the fit over the same sections of flight that we had fitted at 1.0% error tolerance without delay (median prediction error: 1.1%; first, third quartiles: 0.9%, 1.6%; sign test on 46 untied differences: $P < 0.001$; *SI Appendix*, Table S3) and systematically lowered the fitted values of N (median N with delay: 2.3; first, third quartiles: 1.4, 3.4; sign test on 46 untied differences: $P = 0.001$), although the effect size was small (median N of 2.3 vs. 2.6, with and without delay). This was not necessarily surprising, because this simple sensitivity analysis did not amount to modeling the effects of sensorimotor delay, which is likely to be shorter than the 0.2-s delay introduced here to verify the robustness of our conclusions to the ±0.1-s timing uncertainty in our data. Nevertheless, in the absence of data with the time resolution needed to accurately identify any sensorimotor delay, our simulations assuming nominally lag-free PN guidance provided the best available phenomenological model of the data.

Optimization of the Navigation Constant

Strikingly, approximately two-thirds of the fitted values of N fell below the interval $3 \leq N \leq 5$ that is typical of guided missiles (*SI Appendix*, Table S1). Lower navigation constants are avoided in

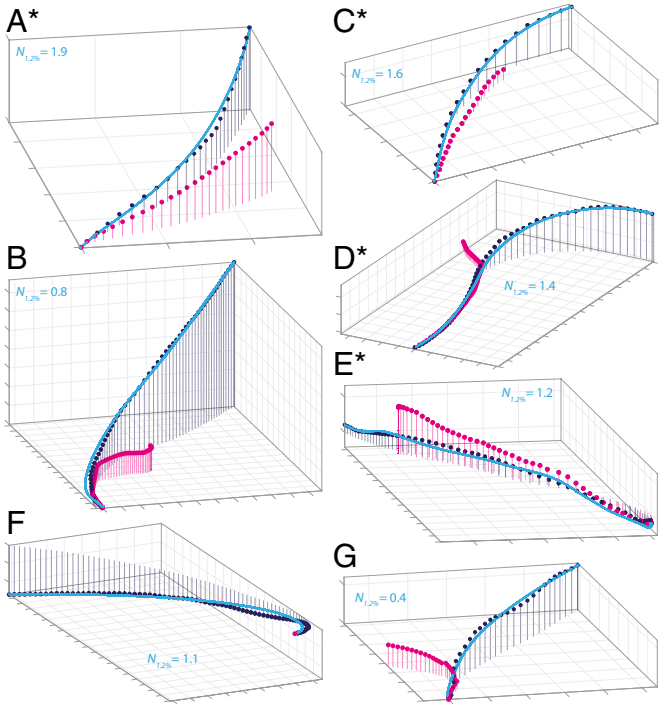

Fig. 5. GPS tracks for peregrines (blue points) attacking maneuvering (*A–E* and *G*) or stationary (*F*) targets (magenta points), overlain with best-fitting 3D simulations under PN guidance (blue lines). Vertical tails end at the horizontal plane in which interception occurs, as an aid to visualization (note that the bird in *F* was flying uphill). Simulations start from the earliest point for which the mean absolute distance between the simulated and measured trajectories was <1.2% (light blue) of the total distance flown; $N_{1.2\%}$ denotes the corresponding best-fitting value of *N*. Starred trajectories are simulated in 3D in Fig. 4 (same lettering). Grid lines are at 10-m spacing.

missile applications, because the acceleration commanded under PN increases without limit at $N < 2$, as the attacker turns ever more tightly in to its target instead of straightening up on final approach (12). The equations that lead to this conclusion are quite involved, but suffice it to say that this textbook result is a fundamental property of the dynamics of PN, such that we might reasonably have expected our peregrines to avoid operating at $N < 2$. In practice, their comparatively low flight speed meant that the centripetal acceleration demanded in our simulations did not exceed gravitational acceleration by more than a factor of 2.5 until the peregrine was already within striking distance of its target. Consequently, the high terminal acceleration demand that can arise at $N < 2$ would never have been limiting for our peregrines. Free of this constraint, it makes good sense that peregrines should operate with lower values of *N* than guided missiles, because PN guidance amplifies errors in line-of-sight rate estimation in proportion to *N*.

The dynamics of PN guidance are highly nonlinear, presenting formidable difficulties analytically. Nevertheless, under linearized lag-free conditions, it can be shown that PN with an effective navigation constant $N' = 3$ is the global optimum for intercepting nonmaneuvering targets, in the sense of being the guidance law which—in a perfect intercept—minimizes the control effort measured by the time integral of the squared acceleration command (12). The effective navigation constant is defined as $N' = N(v\cos\delta)/v_c$, where v_c is the speed at which the attacker closes range on its target. Hence, since $v_c = v\cos\delta$ by definition when the target is stationary, it follows that PN guidance with $N = 3$ will produce the most efficient trajectory possible in terms of the control effort needed to hit a stationary target. This theoretical optimum is remarkably close to the median value of $N_{1.0\%} = 2.6$ that we found empirically for attacks on stationary targets. Against maneuvering targets, the optimal guidance command becomes augmented by a term related to the target's acceleration (12), but as the optimal guidance law in this case is effectively just an augmented form of PN at $N' = 3$, it is striking that we also found a median value of $N_{1.0\%} = 2.6$ for attacks against maneuvering targets. Given that *N* varied substantially between flights (median absolute deviation of $N_{1.0\%}$ from the median: 38% of median), and given that its variation was too great to be attributable to fitting error (median sensitivity ratio of fits: 3.5), it is reasonable to ask whether *N* varied systematically between or within flights. There are good reasons for expecting this. For example, although a fixed navigation constant of $N = 3$ is expected to minimize the control effort for attacks on stationary targets, other performance objectives like minimizing the turn radius or time to intercept could have affected the outcome of the optimization differently, according to the motivation of the attacker or degree of clutter in the environment. Moreover, for attacks on maneuvering targets, the optimal value of *N* is likely to be time-varying in the nonlinear case, and even a flight trajectory generated by the optimal augmented PN law at $N' = 3$ would have appeared to have a time-varying value of *N* when approximated by a trajectory generated by pure PN.

After removing four robustly identified outliers falling >2.5 median absolute deviations from the median (32), the 42 remaining values of $N_{1.0\%}$ were close to normally distributed (Shapiro–Wilk test: $W = 0.96$; $P = 0.13$), so we used an analysis of covariance to test for possible sources of systematic variation in *N* between passes, treating different data points from the same individual as if they were independent. We found no evidence of any effect of target type [serving as a proxy for target acceleration: $F_{(1,39)} = 0.80$; $P = 0.38$] or mean groundspeed [serving as a proxy for motivation level: $F_{(1,39)} = 0.07$; $P = 0.79$] on the fitted values of $N_{1.0\%}$. Testing for systematic variation in *N* within a trajectory risked overfitting, so to test for one mechanistically plausible (albeit functionally suboptimal) pattern of variation within flights, we rewrote the PN guidance law (Eq. **1**) in terms of the centripetal acceleration (a), such that $a(t) = Nv(t)\dot{\lambda}(t)$, and tried fitting the trajectories while holding the gain $Nv(t)$, rather than *N*, constant. This generates a different trajectory if the attacker's speed *v* varies through an attack, and amounts to assuming that the attacker controls its centripetal acceleration (and hence normal aerodynamic force) in proportion to the line-of-sight rate. For 16 of the 55 attack passes, our simulations holding $Nv(t)$ constant fitted a greater duration of flight at 1.0% error tolerance than did the simulations holding *N* constant (cf. 14 cases with the opposite outcome), but this result was not significant (sign test on 30 untied differences: $P = 0.86$), and the simulations holding *N* constant fitted a greater length of flight in aggregate. It would therefore be premature to conclude that peregrines effectively optimize *N* according to their target's or their own behavior, but it is tempting to suppose that they might.

In summary, the median fitted values of $N_{1.0\%}$ fell within just 15% of the optima expected under the classical linear–quadratic formulation of the optimal guidance problem. While the fitted values of *N* were mostly lower than those of guided missiles, they make sense for a biological system flying at comparatively low speeds, for which even the high terminal accelerations associated with $N < 2$ remain tolerable until the attacker is already within striking range of its target. Furthermore, it is reasonable to expect that a biological system will have noisier line-of-sight rate estimation than an engineered system, in which case a lower value of *N* would be expected to be beneficial on the basis that PN propagates errors in line-of-sight rate estimation approximately in proportion to *N* (12). Finally, biological systems usually have longer time constants than engineered systems, and the conditions guaranteeing finite-time stability of PN in the presence of delay (12) imply that a longer time constant can be accommodated by operating at a lower gain (see also ref. 33). Hence, while the variation in the fitted values of *N* remains to be explained, their population properties make excellent functional sense.

Conclusions

Previous research has looked for simple geometric rules describing the aerial attack behaviors of animals (1–11). The attack trajectories of peregrines are not described by any single geometric rule (cf. refs. 7–9), but they are well described by a single form of guidance law—PN—that is capable of producing any of the idealized attack geometries described in nature given appropriate tuning of its navigation constant (Fig. 1 *A*–*C*). This same mechanism, therefore, has the potential to unify our understanding of pursuit behaviors across species—whether in the air, the water, or on the ground. Although peregrines are the first aerial predators for which a guidance law has been formally identified, the fact that other animals such as dragonflies and robber flies tend toward a parallel navigation course on final approach (1–6) is consistent with the hypothesis that they, too, use PN (3, 4, 6). Besides responding effectively to moving targets, PN can be used to steer an energetically optimal approach to a stationary target, correcting simultaneously for steering error and wind drift. It follows that PN could underpin a far wider range of visually guided flight behaviors than the attack behaviors considered here. This hypothesis is mechanistically appealing, because PN does not require any information on target speed or range, merely requiring an estimate of the line-of-sight rate. How this estimate is obtained will depend on the gaze stabilization strategy of the animal: If the head/eyes track the target, then the line-of-sight rate can be obtained from their rotation in an inertial frame; conversely, if the head/eyes are stabilized inertially, then the line-of-sight rate can be obtained from the drift of the target's image across the retina. It remains an open question how peregrines might mechanize PN, but, as the head of a bird plays a role analogous to the gimbaled seeker of a guided missile, with visual and inertial sensors providing the sensory input to both, the missile literature offers useful pointers for future research. Conversely, our results from peregrines point to the fact that PN guidance optimized for low flight speeds could find use in small visually guided drones designed to remove other drones from protected airspace.

Materials and Methods

Experimental Protocol. Each of the $n = 8$ peregrines carried a GPS receiver logging position and groundspeed at 5 Hz (BT-Q1300; Qstarz International) and a forward-facing camera recording 1,280 × 720-pixel video at 30 fps (HD808; Hetai Digital Technology). The camera was worn dorsally on a falconry harness (TrackPack; Marshall Radio Telemetry), while the GPS was mounted on the camera, carried on a tail mount, or worn on the leg jesses. The equipment weighed 0.031 kg in total (<5% body mass). Against stationary targets, the bird was released and allowed to gain height before being called to a food lure thrown upward by the falconer (*SI Appendix*, Fig. S4*A* and Movie S1). Against maneuvering targets (*SI Appendix*, Fig. S4*B* and Movies S2 and S3), the bird was usually allowed to gain height before the aircraft towing the lure was launched, but was sometimes released after the aircraft was airborne. The pilot was instructed to maneuver the aircraft to cause the lure to swing unpredictably. For safety, the lure was released on a parachute upon capture. The protocol was reviewed and approved by the US Air Force, Surgeon General's Human and Animal Research Panel, and the Animal Welfare and Ethical Review Board of the University of Oxford's Department of Zoology.

Data Processing. We screened the GPS data for accuracy and precision (*SI Appendix*), and, after discarding data contaminated by electromagnetic interference from the video camera in one unfortunate mounting configuration, we were left with high-quality GPS data from 23 flights against stationary targets ($n = 3$ birds; 33 passes) and 22 flights against maneuvering targets ($n = 4$ birds; 22 passes). We synchronized the video and GPS data by identifying the start and end of the flight in each data stream and used the video to identify the point of intercept, having interpolated a small number of dropped GPS data points identified by examining their time code. As the thrown targets moved only a short distance horizontally, we identified their position from the GPS coordinates of the bird at the moment it reached its target in the video. For the towed targets, we used another GPS unit attached to the lure to identify the target's trajectory. We then shifted the target's trajectory to align the coordinates of the target and the bird at the known point of intercept, so as to remove any discrepancies arising from inaccuracy in the GPS position estimates.

ACKNOWLEDGMENTS. We thank Martin Cray and Malcolm Beard for falconry and piloting; M. Jones for birds; G. Breakwell, J. Binns, R. Watkins, T. Whittal-Williams, and the Dowlais Top Investment Company Ltd. for land access; Robin Mills for comments; and Eve Richardson for field assistance. This work is based on research sponsored by the Air Force Research Laboratory, under Agreement FA8655-11-1-3065 (to G.K.T. and A.L.R.T.). This project was supported by the European Research Council under the European Union's Horizon 2020 research and innovation program Grant 682501 (to G.K.T.).

1. Mischiati M, et al. (2015) Internal models direct dragonfly interception steering. *Nature* 517:333–338.
2. Mizutani A, Chahl JS, Srinivasan MV (2003) Insect behaviour: Motion camouflage in dragonflies. *Nature* 423:604.
3. Olberg RM (2012) Visual control of prey-capture flight in dragonflies. *Curr Opin Neurobiol* 22:267–271.
4. Olberg RM, Seaman RC, Coats MI, Henry AF (2007) Eye movements and target fixation during dragonfly prey-interception flights. *J Comp Physiol A Neuroethol Sens Neural Behav Physiol* 193:685–693.
5. Olberg RM, Worthington AH, Venator KR (2000) Prey pursuit and interception in dragonflies. *J Comp Physiol A Neuroethol Sens Neural Behav Physiol* 186:155–162.
6. Wardill TJ, et al. (2017) A novel interception strategy in a miniature robber fly with extreme visual acuity. *Curr Biol* 27:854–859.
7. Tucker VA (2000) The deep fovea, sideways vision and spiral flight paths in raptors. *J Exp Biol* 203:3745–3754.
8. Tucker VA, Tucker AE, Akers K, Enderson JH (2000) Curved flight paths and sideways vision in peregrine falcons (*Falco peregrinus*). *J Exp Biol* 203:3755–3763.
9. Kane SA, Zamani M (2014) Falcons pursue prey using visual motion cues: New perspectives from animal-borne cameras. *J Exp Biol* 217:225–234.
10. Kane SA, Fulton AH, Rosenthal LJ (2015) When hawks attack: Animal-borne video studies of goshawk pursuit and prey-evasion strategies. *J Exp Biol* 218:212–222.
11. Ghose K, Horiuchi TK, Krishnaprasad PS, Moss CF (2006) Echolocating bats use a nearly time-optimal strategy to intercept prey. *PLoS Biol* 4:e108.
12. Shneydor NA (1998) *Missile Guidance and Pursuit: Kinematics, Dynamics and Control* (Woodhead, Cambridge, UK).
13. Land MF, Collett TS (1974) Chasing behavior of houseflies (*Fannia canicularis*)–Description and analysis. *J Comp Physiol* 89:331–357.
14. Buelthoff H, Poggio T, Wehrhahn C (1980) 3-D Analysis of the flight trajectories of flies (*Drosophila melanogaster*). *Z Naturforsch* 35c:811–815.
15. Wehrhahn C, Poggio T, Bulthoff H (1982) Tracking and chasing in houseflies (*Musca*)–An analysis of 3-D flight trajectories. *Biol Cybern* 45:123–130.
16. Poggio T, Reichardt W (1981) Visual fixation and tracking by flies: Mathematical properties of simple control systems. *Biol Cybern* 40:101–112.
17. Collett TS, Land MF (1978) How hoverflies compute interception courses. *J Comp Physiol* 125:191–204.
18. Collett TS, Land MF (1975) Visual control of flight behavior in the hoverfly *Syritta pipiens* L. *J Comp Physiol* 99:1–66.
19. Land MF (1993) Chasing and pursuit in the dolichopodid fly *Poecilobothrus nobilitatus*. *J Comp Physiol A Neuroethol Sens Neural Behav Physiol* 173:605–613.
20. Lin H-T, Ros IG, Biewener AA (2014) Through the eyes of a bird: Modelling visually guided obstacle flight. *J R Soc Interface* 11:20140239.
21. Lanchester BS, Mark RF (1975) Pursuit and prediction in the tracking of moving food by a teleost fish (Acanthaluteres spilomelanurus). *J Exp Biol* 63:627–645.
22. Gilbert C (1997) Visual control of cursorial prey pursuit by tiger beetles (Cicindelidae). *J Comp Physiol A Neuroethol Sens Neural Behav Physiol* 181:217–230.
23. Haselsteiner AF, Gilbert C, Wang ZJ (2014) Tiger beetles pursue prey using a proportional control law with a delay of one half-stride. *J R Soc Interface* 11:20140216.
24. Zhang SW, Wang XA, Liu ZL, Srinivasan MV (1990) Visual tracking of moving targets by freely flying honeybees. *Vis Neurosci* 4:379–386.
25. Srinivasan MV, Davey M (1995) Strategies for active camouflage of motion. *Proc Biol Sci* 259:19–25.
26. Justh EW, Krishnaprasad PS (2006) Steering laws for motion camouflage. *Proc R Soc Lond A* 462:3629–3643.
27. O'Rourke CT, Hall MI, Pitlik T, Fernández-Juricic E (2010) Hawk eyes I: Diurnal raptors differ in visual fields and degree of eye movement. *PLoS One* 5:e12802.
28. Anderson EW (1982) Navigational principles as applied to animals. *J Navig* 35:1–27.
29. Jenkins AR (2000) Hunting mode and success of African peregrines *Falco peregrinus minor*: Does nesting habitat quality affect foraging efficiency? *Ibis* 142:235–246.
30. Cresswell W (1996) Surprise as a winter hunting strategy in sparrowhawks *Accipiter nisus*, peregrines *Falco peregrinus* and merlins *F. columbarius*. *Ibis* 138:684–692.
31. Dekker D, Bogaert L (1997) Over-ocean hunting by peregrine falcons in British Columbia. *J Raptor Res* 31:381–383.
32. Leys C, Ley C, Klein O, Bernard P, Licata L (2013) Detecting outliers: Do not use standard deviation around the mean, use absolute deviation around the median. *J Exp Soc Psychol* 49:764–766.
33. Strydom R, Singh SPN, Srinivasan MV (2015) Biologically inspired interception: A comparison of pursuit and constant bearing strategies in the presence of sensorimotor delay. *Proceedings of the 2015 IEEE International Conference on Robotics and Biomimetics* (IEEE, Piscataway, NJ), pp 2442–2448.